

# Sensitivity of future linear $e^+e^-$ colliders to processes of dark matter production with light mediator exchange

Jan Kalinowski<sup>1</sup>, Wojciech Kotlarski<sup>2</sup>, Krzysztof Mękała<sup>1</sup>, Paweł Sopicki<sup>1</sup>,  
and Aleksander Filip Żarnecki<sup>1\*</sup>

<sup>1</sup>*Faculty of Physics, University of Warsaw, Poland*

<sup>2</sup>*Institut für Kern- und Teilchenphysik, TU Dresden, Germany*

<sup>\*</sup>*filip.zarnecki@fuw.edu.pl*

November 2, 2021

## Abstract

As any  $e^+e^-$  scattering process can be accompanied by a hard photon emission from the initial state radiation, the analysis of the energy spectrum and angular distributions of those photons can be used to search for hard processes with an invisible final state. Thus high energy  $e^+e^-$  colliders offer a unique possibility for the most general search of dark matter (DM) based on the mono-photon signature. We consider production of DM particles at the International Linear Collider (ILC) and Compact Linear Collider (CLIC) experiments via a light mediator exchange. Detector effects are taken into account within the DELPHES fast simulation framework. Limits on the light DM production in a simplified model are set as a function of the mediator mass and width based on the expected two-dimensional distributions of the reconstructed mono-photon events. The experimental sensitivity is extracted in terms of the DM production cross section. Limits on the mediator couplings are then presented for a wide range of mediator masses and widths. For light mediators, for masses up to the centre-of-mass energy of the collider, coupling limits derived from the mono-photon analysis are more stringent than those expected from direct resonance searches in decay channels to SM particles.

# 1 Introduction

Excess of mono-photon events is considered as one of possible signatures of DM production at high energy  $e^+e^-$  colliders. One of the advantages of this approach is that the photon radiation from the initial state can be described within the Standard Model and depends only indirectly on the DM production mechanism. Prospects for DM searches at future  $e^+e^-$  colliders were already studied in the past, most recent results for CLIC and ILC are presented in [1, 2] and [3], respectively. However, most of the studies focused on simplified model scenarios where the mediator mass  $M_Y$  was large,  $M_Y \gg \sqrt{s}, \sqrt{|t|}$ , in which case an Effective Field Theory (EFT) description was valid.

Considered in this study is an intermediate mediator mass range, where the mediator might still be resolved at energies accessible at high energy ILC or CLIC. We use results of our recent work [4] for precise modeling of mono-photon processes with WHIZARD [5, 6]. We propose a novel analysis approach where the experimental sensitivity to DM production,  $e^+e^- \rightarrow \chi\chi$ , is studied as a function of the mediator mass and width based on the expected two-dimensional distributions of the reconstructed mono-photon events,  $e^+e^- \rightarrow \chi\chi\gamma$ . Limits presented in terms of the light DM production cross section are expected to be least dependent on the model details.

Mono- and multi-photon events were studied in LEP experiments, for collision energies up to  $\sqrt{s} = 209$  GeV [7–10]. In particular, the observed numbers of mono-photon events were used to set limits on the number of light neutrino flavours. On the other hand, assuming three active neutrino flavours, upper limits of  $\mathcal{O}(100)$  fb were derived on new, exotic processes with production of an invisible final state and a single photon. Experiments at future  $e^+e^-$  colliders will allow to significantly improve these limits and extend them to higher mediator masses.

The paper is structured as follows. In section 2, we describe the simplified model used for modeling DM production processes. In section 3, the framework used for background and signal event simulation is presented as well as the approach used to set limits on the signal cross sections. Constraints on DM production processes expected at 500 GeV ILC and 3 TeV CLIC are discussed in section 4. Section 5 presents our conclusions.

## 2 Computational framework

### 2.1 Simplified DM model

We consider a simplified DM model which covers most popular scenarios of dark matter pair-production at  $e^+e^-$  colliders. In this model the dark matter particles,  $\chi_i$ , couple to the SM particles via the mediator,  $Y_j$ . Each simplified scenario is characterized by one mediator and one dark matter candidate from the set listed in Tab. 1. The interaction between DM and the electrons can be mediated by a real scalar  $Y_R$  or a real vector  $Y_V$ , with the Lagrangian describing mediator coupling to electrons given by

$$\mathcal{L}_{eeY} \ni \bar{e}(g_{eY_R}^1 + i\gamma^5 g_{eY_R}^5)eY_R + \bar{e}\gamma_\mu(g_{eY_V}^1 + \gamma^5 g_{eY_V}^5)eY_V^\mu.$$

Only real values of couplings  $g_{eY_R}^1$ ,  $g_{eY_R}^5$ ,  $g_{eY_V}^1$  and  $g_{eY_V}^5$  are taken into account, and, depending on the coupling choice, six different scenarios are considered in the presented study, as listed in Tab. 2. In addition, five DM candidates can be considered: a real scalar  $\chi_R$ , a complex scalar  $\chi_C$ , a Majorana fermion  $\chi_M$  and a Dirac fermion  $\chi_D$ , and a real vector  $\chi_V$ . We choose to

	particle	mass	spin	charge	self-conjugate
mediator	$Y_R$	$M_{Y_R}$	0	0	yes
	$Y_V$	$M_{Y_C}$	1	0	yes
	$T_C$	$M_{T_C}$	0	1	no
DM	$\chi_R$	$m_{\chi_R}$	0	0	yes
	$\chi_C$	$m_{\chi_C}$	0	0	no
	$\chi_M$	$m_{\chi_M}$	$\frac{1}{2}$	0	yes
	$\chi_D$	$m_{\chi_D}$	$\frac{1}{2}$	0	no
	$\chi_V$	$m_{\chi_V}$	1	0	yes

Table 1: Summary of mediators and DM candidates included in the simplified DM model considered.

scenario	mediator	$g_{eY_R}^1$	$g_{eY_R}^5$	$g_{eY_V}^1$	$g_{eY_V}^5$
Scalar	$Y_R$	$g_{eeY}$	0	0	0
Pseudo-scalar	$Y_R$	0	$g_{eeY}$	0	0
Vector	$Y_V$	0	0	$g_{eeY}$	0
Pseudo-vector	$Y_V$	0	0	0	$g_{eeY}$
V–A coupling	$Y_V$	0	0	$g_{eeY}$	$-g_{eeY}$
V+A coupling	$Y_V$	0	0	$g_{eeY}$	$g_{eeY}$

Table 2: Summary of mediator scenarios considered in the presented study.

investigate the sensitivity of future  $e^+e^-$  colliders in terms of the DM production cross section. For DM particle mass significantly below half of the mediator mass, pair-production cross section can be given in terms of the mediator partial widths (to electrons and DM particle), its total width and mass. Since we assume that the total width is dominated by the DM partial width, cross section dependence on the DM particle couplings is absorbed in the total mediator width and the limits extracted for fixed mediator mass and width hardly depend on the DM particle type or coupling structure. Therefore, only the Dirac fermion,  $\chi_D$ , is considered as the DM particle, and its interactions with possible mediators are described by

$$\mathcal{L}_{\chi\chi Y} \ni \bar{\chi}_D(g_{\chi_D Y_R}^1 + \nu\gamma^5 g_{\chi_D Y_R}^5)\chi_D Y_R + \bar{\chi}_D\gamma_\mu(g_{\chi_D Y_V}^1 + \gamma^5 g_{\chi_D Y_V}^5)\chi_D Y_V^\mu,$$

where, for simplicity, for each scenario described in Tab. 2 the structure of mediator couplings to DM fermions is assumed to be the same as to SM fermions. The DM particle type and its coupling structure becomes relevant only when the cross section limits are translated to the limits on the product of mediator couplings.<sup>1</sup> Moreover, to simplify the discussion in terms of the mediator properties, we fix the mass of the DM fermion to  $m_\chi = 50 \text{ GeV}$  throughout the paper.<sup>2</sup> On the other hand, if an excess of mono-photon events is observed, determination of the DM type and coupling structure affecting the observed photon distribution is possible [11], which however goes beyond the scope of the current study.

<sup>1</sup>For example, limits on the product of mediator couplings,  $g_{eeY}g_{\chi\chi Y}$ , presented in Sec. 4 decrease by a factor of  $\sqrt{2}$ , if Majorana fermion DM is assumed.

<sup>2</sup>For light mediator scenarios, DM particle mass has marginal impact on the analysis results as long as it is significantly below half of the mediator mass.

The model defined by the Lagrangian described above, also including other DM particle types shown in Tab. 1, has been encoded into FEYNRULES [12, 13] and exported in UFO format [14], which was then used as an input to WHIZARD [5, 6]. More details as well as the UFO file of the model can be found in [15].

## 2.2 Theoretical and experimental constraints

This study focuses on scenarios where the mediator might be produced on-shell at energies accessible at high energy ILC or CLIC. For the validity of the cross section calculations and event sample generation in WHIZARD (see sec. 3.1), we have to assume that the total width of the mediator is smaller than its mass (so the mediator itself is well defined as a particle) and its couplings are small (so perturbative approach is applicable). The first condition is fulfilled by fixing the ratio of mediator width to mediator mass in the considered analysis scenarios and restricting the study to the range  $\Gamma/M \leq 0.5$ . To ensure validity of perturbative calculations and to respect the experimental constraints described below, coming from LEP and LHC experiments, we assume mediator coupling to electrons of  $g_{eeY} = 0.01$  for reference cross section calculations and signal sample generation.

Radiative DM pair-production scenario described above was not addressed in the analysis of mono-photon events at LEP [7–10]. However, limits on the mono-photon production cross section at  $\sqrt{s} = 205$  GeV presented in [8] can be compared with generator-level predictions of our model. Limits of 50–150 fb on the cross section for single photon production in the central detector region,  $45^\circ < \theta_\gamma < 135^\circ$ , correspond to the limits on the mediator coupling to electrons of the order of 0.01–0.02 extending almost up to the kinematic limit,  $M_Y \leq 200$  GeV.

The strategy employed by ATLAS and CMS is to show exclusion limits in the DM mass versus mediator mass plane for selected benchmark scenarios proposed in [16]. For light DM states, results from the ATLAS collaboration [17], looking for the dark matter production in association with an energetic photon at  $\sqrt{s} = 13$  TeV, exclude mediator masses up to 920–1470 GeV, depending on the scenario. However, scenarios [16] assume relatively strong mediator coupling to quarks,  $g_{qqY} = 0.1$  or 0.25. For quark coupling values below 0.03, no constraints on the light mediator scenarios can be set in any of the considered analysis approaches [18]. Also CMS results [19] on the resonance search in high-mass dilepton final states at  $\sqrt{s} = 13$  TeV indicate that mediator masses up to about 3 TeV can be excluded for large mediator coupling values to quarks and leptons,  $g_{qqY} = g_{llY} = 0.1$ . However, for weaker lepton coupling,  $g_{llY} = 0.01$ , scenarios with light DM particle and mediator mass below 1 TeV are still not excluded.

## 2.3 Search strategy

We propose a novel approach to the DM searches at colliders, where the experimental sensitivity is defined in terms of both the mediator mass and mediator width. Limits on the light DM production cross section can be set based on the two-dimensional distributions of the reconstructed mono-photon events. This approach is more model independent than the approaches presented so far, in which given mediator coupling values to SM and DM particles were assumed. Also, as the observed photons predominantly come from initial state radiation, extracted cross section limits hardly depend on the details of the BSM scenario.

To simplify the presentation, we consider models with fixed ratio of mediator width to mediator mass. We consider “narrow” mediator scenarios with  $\Gamma/M = 0.01$  and 0.03, “medium”

with  $\Gamma/M = 0.1$  and “wide” with  $\Gamma/M = 0.5$ . We assume that the mediator coupling to SM particles is small (the reference coupling value is 0.01) so that mediator decays to SM particles can be neglected. Our results (cross section limits for invisible decays) remain valid also for the case when decays to SM particles would be visible, but the analysis based on combination of visible and invisible decay channels is beyond the scope of this study.

## 2.4 Linear collider running scenarios

The baseline running scenario for the ILC assumes the integrated luminosities of about  $2 \text{ ab}^{-1}$  at 250 GeV and  $4 \text{ ab}^{-1}$  at 500 GeV, with an additional  $200 \text{ fb}^{-1}$  collected at the top-quark pair-production threshold around 350 GeV [20]. The accelerator design allows for polarisation of both  $e^-$  and  $e^+$  beams, of 80% and 30%, respectively. The H-20 running scenario for ILC was proposed in [21], to optimise the physics performance of the experiment. It assumes that 80% of the total integrated luminosity at 500 GeV will be collected with opposite beam polarisations ( $1600 \text{ fb}^{-1}$  for left-handed electrons and right-handed positrons,  $e_L^- e_R^+$ , and  $1600 \text{ fb}^{-1}$  for  $e_R^- e_L^+$  running, denoted as LR and RL configurations in the following) and 20% with same polarisations of both beams ( $400 \text{ fb}^{-1}$  for  $e_L^- e_L^+$  and  $400 \text{ fb}^{-1}$  for  $e_R^- e_R^+$  running, referred to as LL and RR runs).

The implementation plan for CLIC [22] assumes collecting  $1 \text{ ab}^{-1}$  at the first construction stage with an energy of 380 GeV, while  $2.5 \text{ ab}^{-1}$  and  $5 \text{ ab}^{-1}$  are expected to be collected for the second and third construction stages, at 1.5 TeV and 3 TeV. Only the electron beam polarisation of 80% is included in the CLIC baseline design. It is assumed that 80% of the integrated luminosity at the 3 TeV stage ( $4 \text{ ab}^{-1}$ ) will be collected with negative (left-handed) electron beam polarisation and 20% ( $1 \text{ ab}^{-1}$ ) with positive polarisation (right-handed electrons).

Sensitivity of linear  $e^+e^-$  collider experiments to DM pair-production is expected to increase with collision energy, both because of the increased mass range for the on-shell mediator production and of the assumed increase in the integrated luminosity. Therefore, considered in the presented study are ILC and CLIC running at the energy stages of 500 GeV and 3 TeV, respectively.

## 2.5 Model predictions

Shown in Fig. 1 is the cross section for DM production,  $e^+e^- \rightarrow \chi\chi$ , as a function of the  $e^+e^-$  collision energy. Pair-production of light Dirac DM,  $m_\chi = 50 \text{ GeV}$ , is considered for scenario with the vector mediator of 300 GeV and different mediator widths, as described above. Possible beam polarisation and beam energy spectra are not taken into account. Large enhancement of DM production is possible for “narrow” mediator scenario, when the beam energy is tuned to the mediator mass. For “light” mediator scenarios, when the collision energy is much higher than the mediator mass,  $M_Y \ll \sqrt{s}$ , production cross section decreases as  $1/s$ .

In the following, we consider scenarios with light mediator and those for which the mediator mass and collision energy are comparable. Shown in Fig. 2 are the expected cross sections for DM production at 500 GeV ILC and 3 TeV CLIC, as a function of the assumed mediator mass for different fractional mediator widths. It is interesting to note that for scenarios with light mediator the production cross section depends very weakly on the mediator mass. Also indicated in Fig. 2 is the impact of the collider luminosity spectra on the expected DM production cross section. At the ILC the effect of the luminosity spectra is significant only for the “narrow”

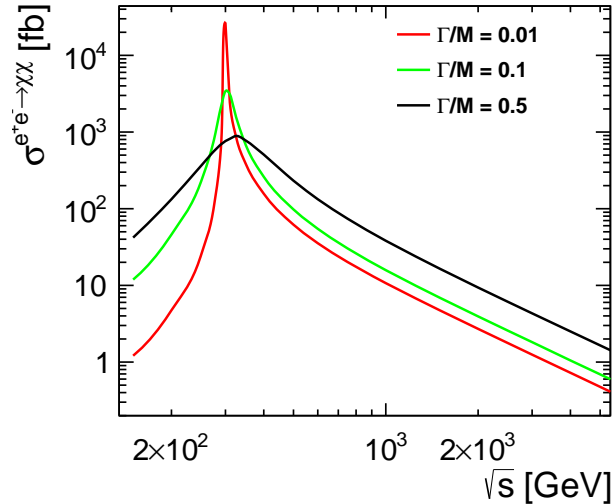


Figure 1: Cross section for DM production in  $e^+e^-$  collisions as a function of the collision energy  $\sqrt{s}$ . Expectations for pair production of light Dirac DM ( $m_\chi = 50$  GeV) are shown for the scenario with vector mediator of 300 GeV and different mediator widths, as indicated in the plot. The mediator coupling to electrons is set to 0.01.

mediator scenario and in the vicinity of the resonance. It is much more important at CLIC where, due to the large contribution of the low energy tail in the beam energy spectra, the cross section for light DM production with exchange of light mediator is significantly enhanced, up to about a factor of 5.

### 3 Data Simulation and Analysis

#### 3.1 Whizard simulation

Main SM background contributions to searches based on mono-photon signature are expected to come from the radiative neutrino pair production,  $e^+e^- \rightarrow \nu\nu\gamma$ , and the radiative Bhabha scattering,  $e^+e^- \rightarrow e^+e^-\gamma$ . For precise kinematic description of photons entering the detector, hard photon emission should be included directly in the matrix element (ME) calculation. On the other hand, very soft and collinear photons should still be simulated with the parametric approach, taking into account proper resummation of higher order corrections. The procedure proposed in [4] allows for consistent, reliable simulation of mono-photon events in WHIZARD [5, 6] for both BSM signal and SM background processes, based on merging the ME calculations with the lepton ISR structure function. Two variables, calculated separately for each emitted photon, are used to describe kinematics of the emission [4]:

$$\begin{aligned} q_- &= \sqrt{4E_0 E_\gamma} \cdot \sin \frac{\theta_\gamma}{2}, \\ q_+ &= \sqrt{4E_0 E_\gamma} \cdot \cos \frac{\theta_\gamma}{2}, \end{aligned}$$

where  $E_0$  is the nominal electron or positron beam energy, while  $E_\gamma$  and  $\theta_\gamma$  are the energy and scattering angle of the emitted photon in question. For the single photon emission they would

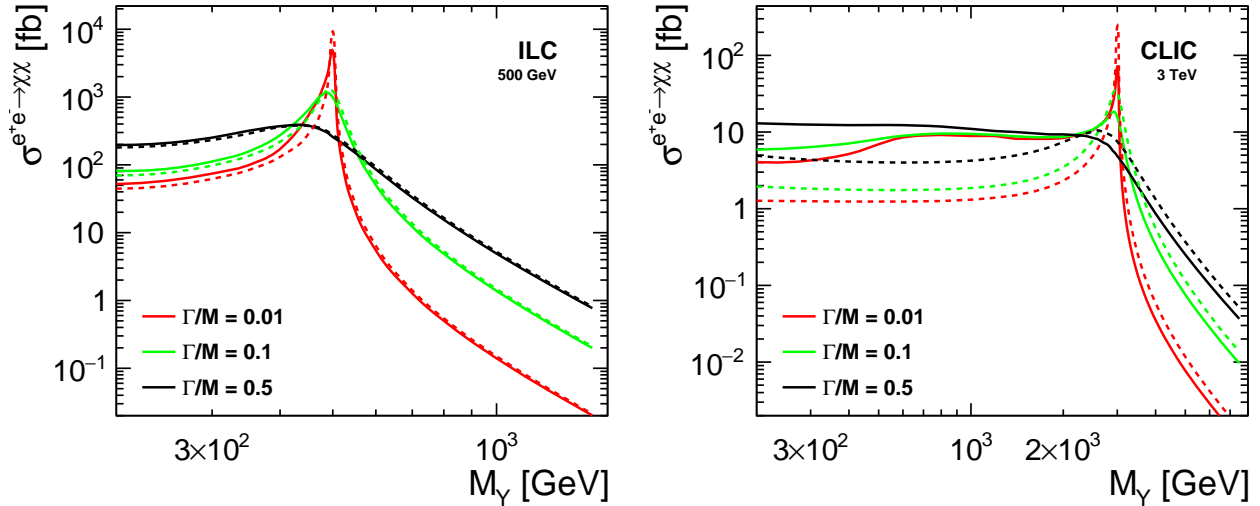


Figure 2: Cross sections for DM production at 500 GeV ILC (left) and 3 TeV CLIC (right) as a function of the assumed mediator mass,  $M_Y$ . Expectations for pair production of light Dirac DM ( $m_\chi = 50$  GeV) are shown for scenario with vector mediator and different fractional mediator widths, as indicated in the plot. Results obtained with the expected collider luminosity spectra taken into account (solid lines) are compared with results assuming monochromatic beam (dashed lines). Mediator coupling to electrons is set to 0.01.

correspond to the virtuality of the electron or positron after (real) photon emission. They are introduced to define the phase-space region where the radiated photon can be reconstructed in the detector, as shown in Fig. 3. Detector acceptance indicated in the plot corresponds to the considered detector models, see Sec. 3.2. Only photons with large values of virtualities  $q_-$  and  $q_+$  can be measured in the detector. We therefore require photons generated at the ME level to have energy above  $E_{min} = 1$  GeV and  $q_\pm$  virtualities above the merging scale  $q_{min} = 1$  GeV. At the same time, to avoid double counting, we reject the events with any of the ISR photons passing the ME photon selection cuts.

Only radiative events were simulated for SM background processes. For 500 GeV ILC (3 TeV CLIC) we require at least one ME photon to be emitted above  $5^\circ$  ( $7^\circ$ ) from the beam axis and with a transverse momentum higher than 2 GeV (5 GeV). After the hard photon selection described above, contribution to the radiative cross section from processes with three ME photons is at per-cent level [4]. Processes with up to three ME photons have been thus included to match the expected precision of the measurement. Contribution from higher order processes is at the level of  $10^{-5}$  and has been neglected.

For the considered DM pair-production scenarios, generated signal samples included both non-radiative and radiative processes (up to three ME photons) to ensure proper evaluation of the total production cross section. The ISR rejection procedure has much stronger impact on the signal generation than for the SM background, resulting in rejection of up to 50% of generated events, as shown in Fig. 4. Highest fraction of events is rejected for low mediator masses and small mediator widths, when radiative return to the mediator mass results in a significant enhancement of the radiative cross section. On the other hand, for the resonant mediator production at nominal collision energy,  $M_Y \approx \sqrt{s}$ , photon radiation is significantly suppressed, and so the number of rejected events is much smaller.



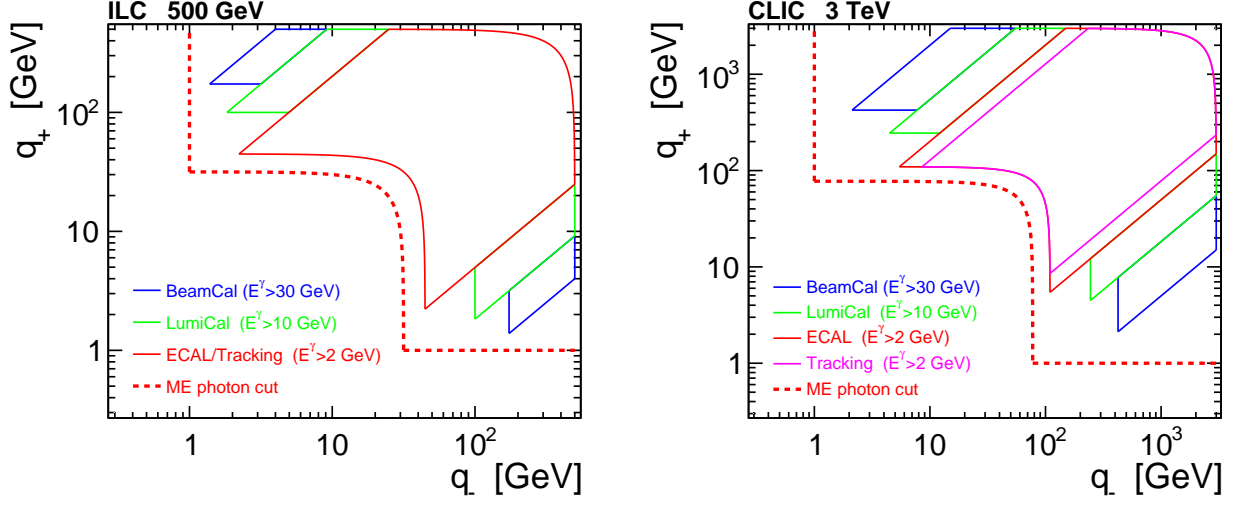


Figure 3: Detector acceptance in the  $(q_+, q_-)$  plane expected for the future experiments at 500 GeV ILC (left) and 3 TeV CLIC (right). Red dashed lines indicate the cut used to restrict the phase space for ME photon generation.

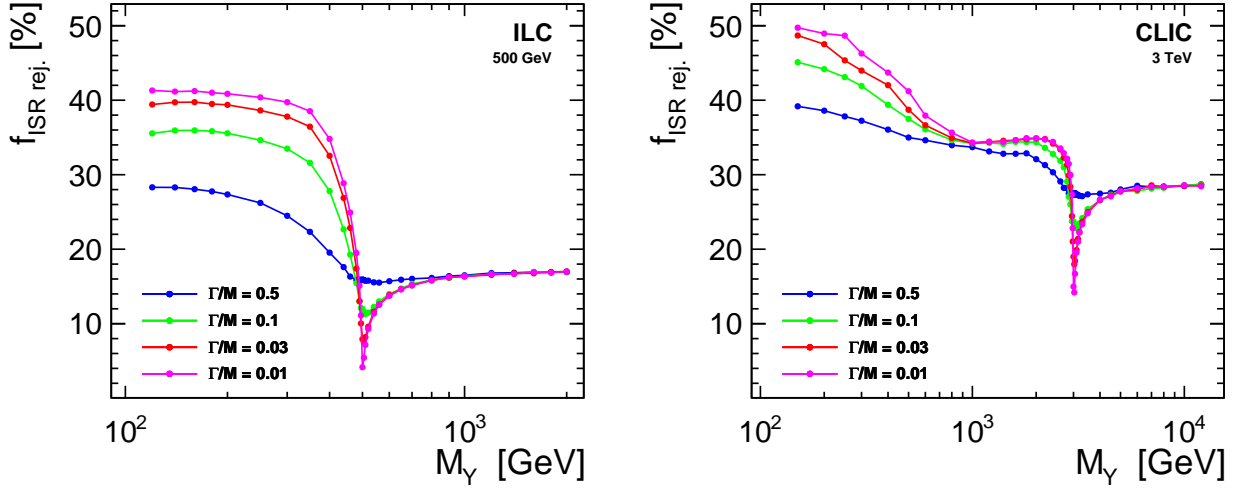


Figure 4: Fraction of WHIZARD events, which are removed by the ISR rejection procedure, as described in [4]. See text for details.



### 3.2 Detector simulation

Results presented in our previous work [4] were based on simple acceptance cuts applied at the generator level. Only the expected geometrical acceptance of the detector was taken into account, while the reconstruction efficiency and the detector resolution was not considered. Proper description of the reconstruction efficiency for electrons scattered at low angles is crucial for the proper modeling of the background coming from the radiative Bhabha scattering [3]. We therefore use the fast simulation framework DELPHES [23] in which the two detector models were implemented recently: `ILCgen` for ILC running at 500 GeV and `CLICdet_Stage3_fcal`, the extended version of `CLICdet_Stage3` [24], for 3 TeV CLIC. Both models include description of the calorimeter systems in the very forward region: the luminosity calorimeter (LumiCal) and the beam calorimeter (BeamCal). Their angular acceptance extends down to 6 mrad for ILC and 10 mrad for CLIC. Implemented in the DELPHES detector models are the reconstruction efficiencies and detector resolutions expected from the full simulation results [25–27].

### 3.3 Event selection

For processes of DM pair-production, we expect radiative photons to be the only final state particles in the detector. The same signature (but with different kinematic distribution) is expected for the SM background coming from the radiative neutrino pair-production. However, the situation is very different for the radiative Bhabha scattering. Transverse momentum of the radiated photon has to be balanced by a scattered electron or another photon.

Photons can be reconstructed with high efficiency and high purity only in the central part of the detector, as the tracking detectors are required to distinguish between photons and electrons (or positrons). To suppress the Bhabha contribution we assume that we should observe only a single photon in the central detector region and no other deposits or tracks. The mono-photon acceptance region in photon rapidity and transverse momentum plane is defined as  $|\eta_\gamma| < 2.8$ ,  $p_T^\gamma > 3$  GeV for 500 GeV ILC and  $|\eta_\gamma| < 2.6$ ,  $p_T^\gamma > 10$  GeV for 3 TeV CLIC. Shown in Fig. 5 are the expected photon energy distributions for selected mono-photon events, for ILC running with LR and RL beam polarisations. Generator level distributions (without mono-photon selection) are shown for comparison. While the selection cuts hardly affect the spectra for radiative neutrino pair-production events,<sup>3</sup> Bhabha background is significantly suppressed. After the selection cuts, which include veto based on BeamCal and LumiCal response, Bhabha scattering background is limited to low photon transverse momentum values. SM background to mono-photon events with high photon transverse momenta is dominated by radiative neutrino pair-production.

As already mentioned above, both non-radiative and radiative processes were included in the signal sample generation. While about half of events included photon generated at the ME level, only a small fraction of those pass the detector acceptance cuts. In Fig. 6, fraction of signal events, which are reconstructed as mono-photon events in the detector is shown as a function of the assumed mediator mass. Signal selection efficiency of 10–15% is obtained for low mass scenarios,  $M_Y \ll \sqrt{s}$ , while for heavy mediator scenarios,  $M_Y \gg \sqrt{s}$ , only about 5% of events can be tagged. Similarly to what was observed in Fig. 4, signal selection efficiency is significantly reduced (following the probability of hard photon radiation) for resonant mediator production,  $M_Y \approx \sqrt{s}$ .

---

<sup>3</sup>For highest photon energy values,  $E_\gamma \approx 250$  GeV, numbers of events after selection cuts are higher than

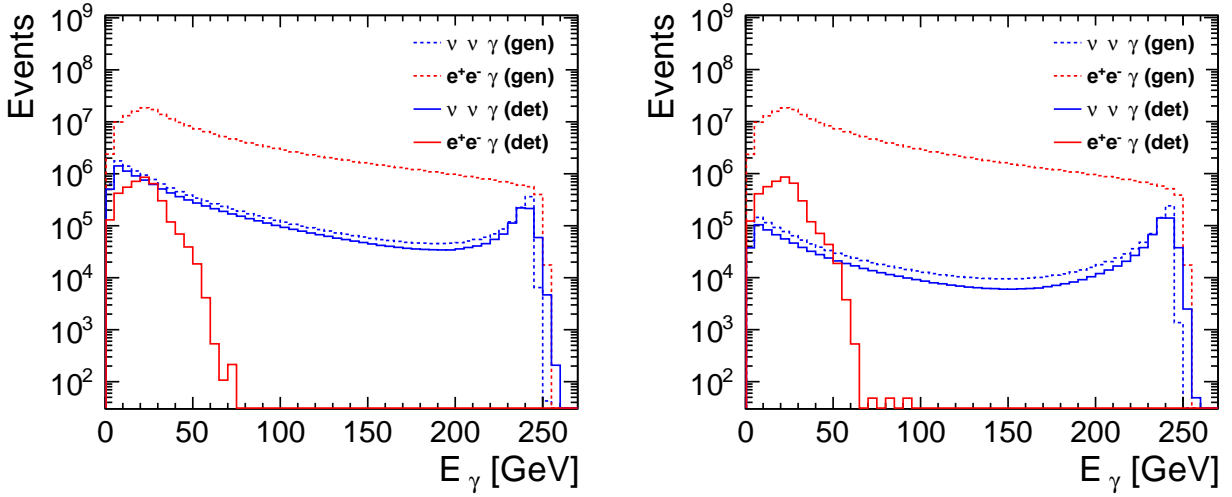


Figure 5: Energy distributions for central photons emitted in radiative neutrino pair production events and radiative Bhabha events. Distributions expected for selected mono-photon events, after detector response simulation with DELPHES (solid lines), are compared with generator level results from WHIZARD (dashed lines). Numbers of events presented correspond to the integrated luminosity of  $1.6 \text{ ab}^{-1}$ , for ILC running at 500 GeV with electron/positron beam polarisation of  $-80\%/+30\%$  (left) and  $+80\%/-30\%$  (right).

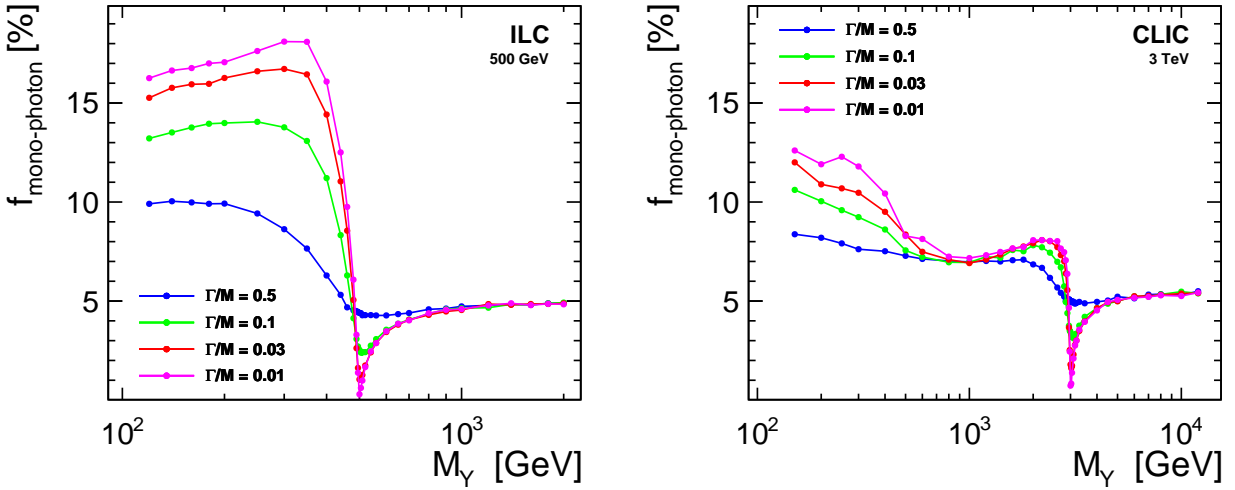


Figure 6: Fraction of dark matter pair-production events, which are reconstructed as mono-photon events in the detector, as a function of the assumed mediator mass, for the ILC running at 500 GeV (left) and CLIC running at 3 TeV (right) and different fractional mediator widths, as indicated in the plot.

### 3.4 Procedure for setting limits

Mono-photon events can be described by just two variables: photon energy and its polar angle or rapidity. We consider 2-D kinematic distributions of mono-photon events in rapidity and transverse momentum fraction  $f_T^\gamma$  defined as

$$f_T^\gamma = \frac{\log\left(\frac{p_T^\gamma}{p_T^{min}}\right)}{\log\left(\frac{p_T^{max}}{p_T^{min}}\right)},$$

where  $p_T^{min}$  is the minimum photon transverse momentum required in the event selection procedure (3 GeV at 500 GeV ILC and 10 GeV at 3 TeV CLIC; see Sec. 3.3) and  $p_T^{max}$  is the maximum transverse momentum of the photon allowed for the given scattering angle

$$p_T^{max} = \frac{\sqrt{s}}{2} \sin \theta_\gamma.$$

Such a choice of variables results in a rectangular phase space region covered by the accepted mono-photon events and reduces the impact of statistical fluctuations. Shown in Fig. 7 is the rapidity vs transverse momentum fraction distributions for mono-photon events expected for SM background processes at 500 GeV ILC and 3 TeV CLIC. Background from radiative Bhabha events remaining after mono-photon selection contributes mainly to the region of low  $f_T^\gamma$  (low transverse momentum) and large photon rapidities while radiative neutrino production dominates the large  $f_T^\gamma$  region. The visible difference in the expected background shape for the ILC and CLIC is mainly due to the fact that the cross section for radiative Bhabha scattering decreases fast with energy and the radiative neutrino pair production cross section increases [4]. Corresponding distributions for examples of signal scenarios are shown in Fig. 8. The shape of the expected signal distribution is very different from that for the SM background. There is a clear ridge visible, corresponding to radiative return events, when the mediator is produced on-shell. We use these 2-D distributions as an input for building measurement model in RooFit [28] and calculate the expected 95% C.L. cross section limits for radiative DM pair-production in the CL<sub>S</sub> approach [29].

### 3.5 Impact of beam polarisation

While the final results from the analysis will be presented only for combined analysis of all runs, taken with different beam polarisation settings, it is important to understand the impact of the beam polarisation on the experimental sensitivity. Shown in Fig. 9 are the expected limits on the radiative light DM pair-production cross section at 500 GeV ILC for four<sup>4</sup> mediator scenarios and different polarisation configurations considered. Running with right-handed electron beam polarisation and left-handed positrons (RL configuration) results in smallest background from neutrino radiative pair-production and thus also the strongest limits for most of the considered scenarios: Scalar, Vector and V+A coupling structure. However, for scenario with V-A coupling structure data collected with LR polarisation configuration is expected to provide much stronger limits. This demonstrates that the optimal choice of the beam polarisation depends

---

numbers of generated events in given energy bin due to detector resolution effects.

<sup>4</sup>Six scenarios are defined in Tab. 2. However, polarisation dependences are not shown for Pseudo-scalar and Pseudo-vector scenarios as they are very similar to those observed for Scalar and Vector scenarios, respectively.

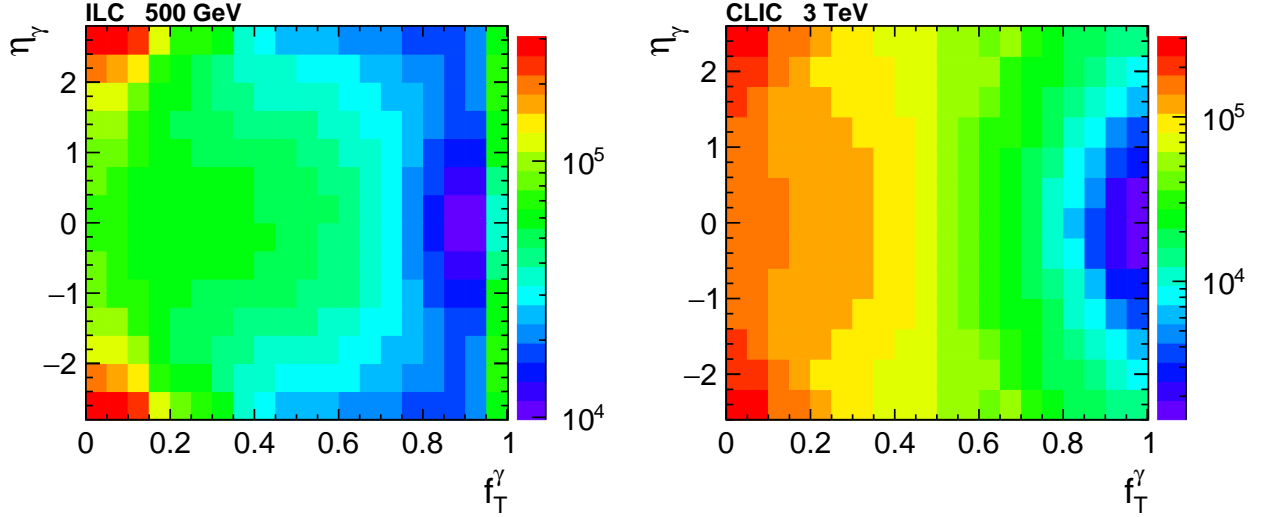


Figure 7: Pseudorapidity vs transverse momentum fraction for mono-photon background events at 500 GeV ILC (left) and 3 TeV CLIC (right). Standard model expectations are normalised to integrated luminosity of  $1600 \text{ fb}^{-1}$  for ILC running with  $-80\%/+30\%$  electron/positron beam polarisation and  $1000 \text{ fb}^{-1}$  for CLIC running with  $-80\%$  electron beam polarisation only.

on the assumed mediator coupling structure and combined analysis of the data collected for all polarisation combinations is required to set most stringent limits for all considered coupling scenarios. Same conclusion holds also for the CLIC running scenarios.

### 3.6 Systematic uncertainties

With high numbers of the expected background events, see Fig. 7, statistical uncertainties of the measurement are expected to be on a sub-percent level. Therefore, possible sources of systematic uncertainties have to be taken into account. When different data sets are combined, it is also very important to take possible correlations in systematic deviations into account. Systematic variations and their correlations were included in the definition of the measurement model in the RooFit framework.

In our choice of systematic effects we follow the approaches adopted in [2, 3]. The following sources of systematic uncertainties were considered in the presented study:

- neutrino background normalisation;  
We assume that the SM predictions for the radiative neutrino pair-production background normalisation are known with relative uncertainty of 0.2% [2] (for both ILC and CLIC). This includes the uncertainty in theoretical predictions as well as the possible uncertainty in the event selection efficiency. The uncertainty is 100% correlated between different data sets.
- Bhabha background normalisation;  
Most of Bhabha background events are removed by selection cuts, vetoes applied based on BeamCal and LumiCal response in particular. High rejection efficiency results in

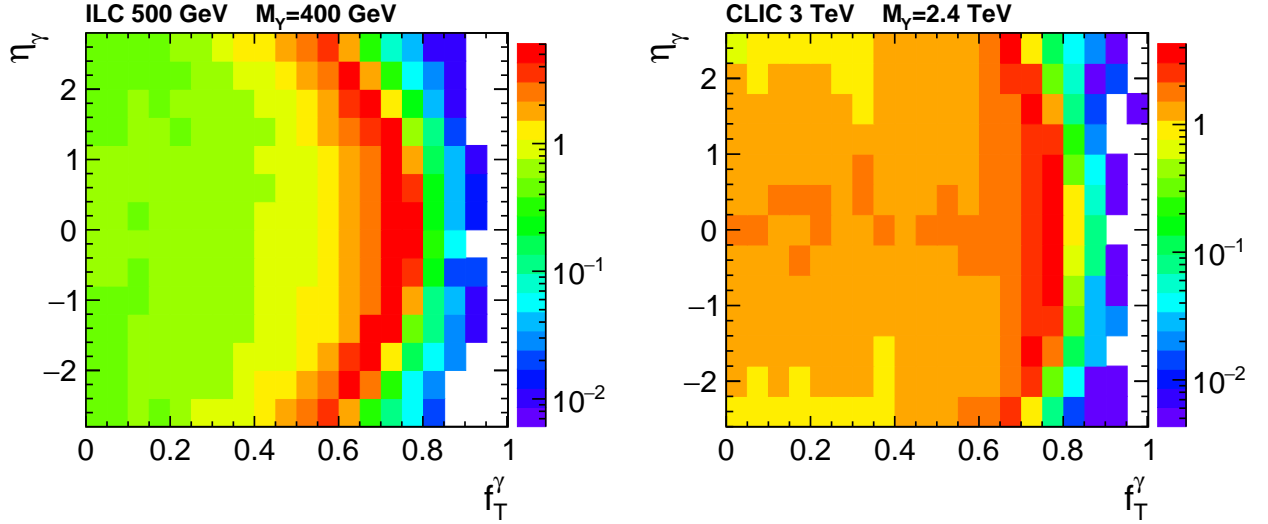


Figure 8: Pseudorapidity vs transverse momentum fraction for mono-photon signal events at 500 GeV ILC (left) and 3 TeV CLIC (right). Pair-production of fermion DM particles with  $m_\chi = 50$  GeV is considered for mediator mass  $M_Y = 400$  GeV at 500 GeV ILC running with  $-80\%/+30\%$  electron/positron beam polarisation (left) and for  $M_Y = 2.4$  TeV at 3 TeV CLIC running with  $-80\%$  electron beam polarisation only (right). Simplified DM model predictions are calculated for the relative mediator width of  $\Gamma/M = 0.03$  and normalised to the unpolarised DM production cross section of 1 fb.

an increased relative uncertainty at the level of accepted events. We assume that the predictions for the Bhabha event background are known to 1% [2] (for both ILC and CLIC). This includes the uncertainty in theoretical predictions as well. The uncertainty is 100% correlated between different data sets.

- integrated luminosity of the data samples;  
We assume 0.26% luminosity uncertainty for 500 GeV ILC [30] and 0.2% uncertainty for 3 TeV CLIC [31]. We consider this uncertainty as uncorrelated between different data sets.
- beam polarisation;  
We assume relative uncertainty on the beam polarisation at ILC of 0.02–0.08%, following approach of [32]. Uncertainties are correlated between runs with the same electron or positron beam polarisation. For CLIC, uncertainty of 0.2% is assumed for the electron beam polarisation [33] (uncorrelated).
- shape of the luminosity spectra;  
We consider possible variation of the luminosity spectra shape by reweighting the signal and background events accordingly. Results of [3] were used for ILC, with systematic variation of spectra normalisation of up to 50% at half of the nominal centre-of-mass energy ( $\sqrt{s'} = \frac{1}{2}\sqrt{s}$ ). We use the same approach for spectra shape uncertainty at CLIC. However, as the low energy tail of the luminosity spectra is much higher at CLIC than at ILC, we assume that its relative uncertainty is an order of magnitude lower and cor-

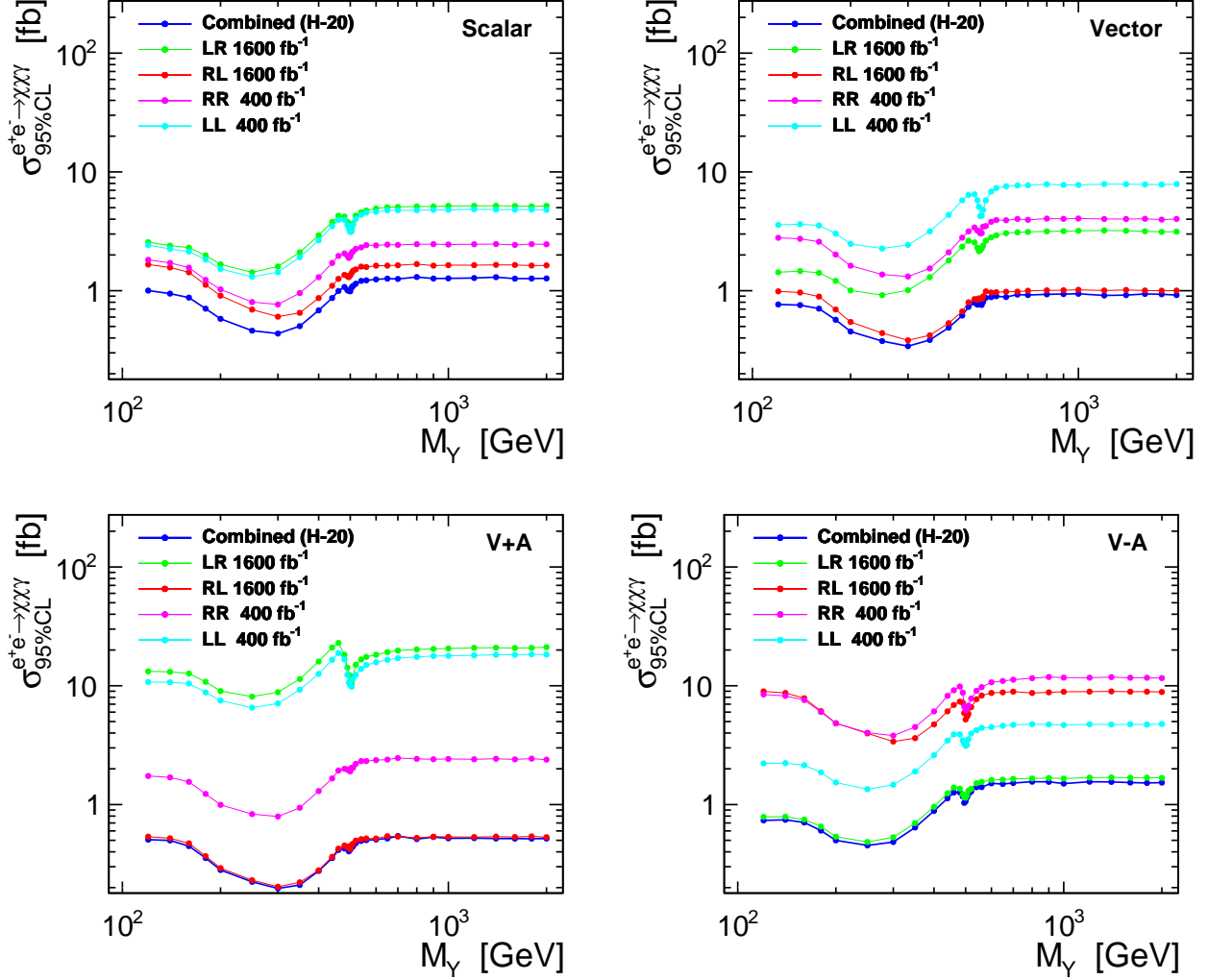


Figure 9: Limits on the cross section for the radiative light DM pair-production processes with  $s$ -channel mediator exchange for 500 GeV ILC. Different mediator coupling scenarios are considered, as indicated in the plot label (see Tab. 2 for details). Limits resulting from running with different beam polarisations and the combined limits are presented. Systematic uncertainties are not taken into account.

responds to 5% normalisation uncertainty at half of the nominal centre-of-mass energy. This uncertainty is 100% correlated between different data sets.

The influence of the systematic uncertainties on the analysis results is illustrated in Fig. 10. Expected limits on the radiative DM pair-production cross section with vector mediator exchange are presented for 500 GeV ILC and 3 TeV CLIC without and with systematic uncertainties taken into account. Impact of systematic uncertainties is most significant for heavy mediator exchange, for  $M_Y > \sqrt{s}$ . When systematic effects are taken into account, expected CLIC combined limits increase by about a factor of 2, with largest contribution coming from the polarisation uncertainty. For ILC, the systematic uncertainties increase the expected combined limits for heavy mediator scenarios by about 40%, with largest contributions coming from the integrated luminosity and spectra shape uncertainties.

## 4 Results

Presented in Fig. 11 are the expected limits on the cross section for radiative DM pair-production at 500 GeV ILC and 3 TeV CLIC, assuming combined analysis of all collected data, as described in sec. 2.4. Limits are presented for the Vector mediator scenario as a function of the mediator mass for different mediator widths, for the Dirac fermion DM with mass  $m_\chi = 50$  GeV. For heavy mediator scenarios,  $M_Y \gg \sqrt{s}$ , expected cross section limits do not depend on the assumed mediator width and weakly depend on the assumed mediator mass. For lower masses, the cross section limits improve and the expected sensitivity is highest, as expected, for narrow mediator scenarios. Surprisingly, the shape of the mass dependence below the resonant production threshold is very different for ILC and CLIC. This can be understood as an effect of the much wider luminosity spectra at CLIC significantly enhancing the resonant production cross section for  $M_Y < \sqrt{s}$ , as already observed in Fig. 2. For ILC running at 500 GeV, the best limits are obtained for resonance with  $M_Y \approx \frac{1}{2}\sqrt{s}$ , while lowest mediator masses are constrained best for CLIC. Still, one should note that the presented 95% C.L. limits on the radiative DM pair-production depend rather weakly on the mediator mass and width, while they change by more than an order of magnitude. The limits are of the order of 1 fb, ranging from about 0.3 fb to 3 fb.

Limits presented in Fig. 11 correspond to processes with hard photon reconstructed in the detector and are therefore sensitive to detector design and analysis details (e.g. the photon transverse momentum or energy thresholds applied). To be able to constrain different BSM scenarios, the limits need to be corrected for the photon tagging efficiency, as discussed in sec. 3.3 and shown in Fig. 6. Resulting limits on the total DM pair-production cross section at 500 GeV ILC and 3 TeV CLIC are presented in Fig. 12. As expected, sensitivity to models with  $M_Y \approx \sqrt{s}$  is significantly reduced except for the very wide mediator scenario. In general, expected limits on the DM pair-production with light mediator exchange are of the order of 10 fb for both ILC and CLIC.

Compared in Fig. 13 are the expected limits on the total DM pair-production cross section at 500 GeV ILC and 3 TeV CLIC, for relative mediator width of  $\Gamma/M = 0.03$  and different mediator coupling scenarios, as listed in Tab. 2. It is interesting to note that for processes with light mediator exchange the model dependence of the total cross section limits is weaker than for the heavy mediator case. Also, running scenario assumed for CLIC, with 80% of integrated luminosity devoted to running with the negative electron beam polarisation (with higher back-



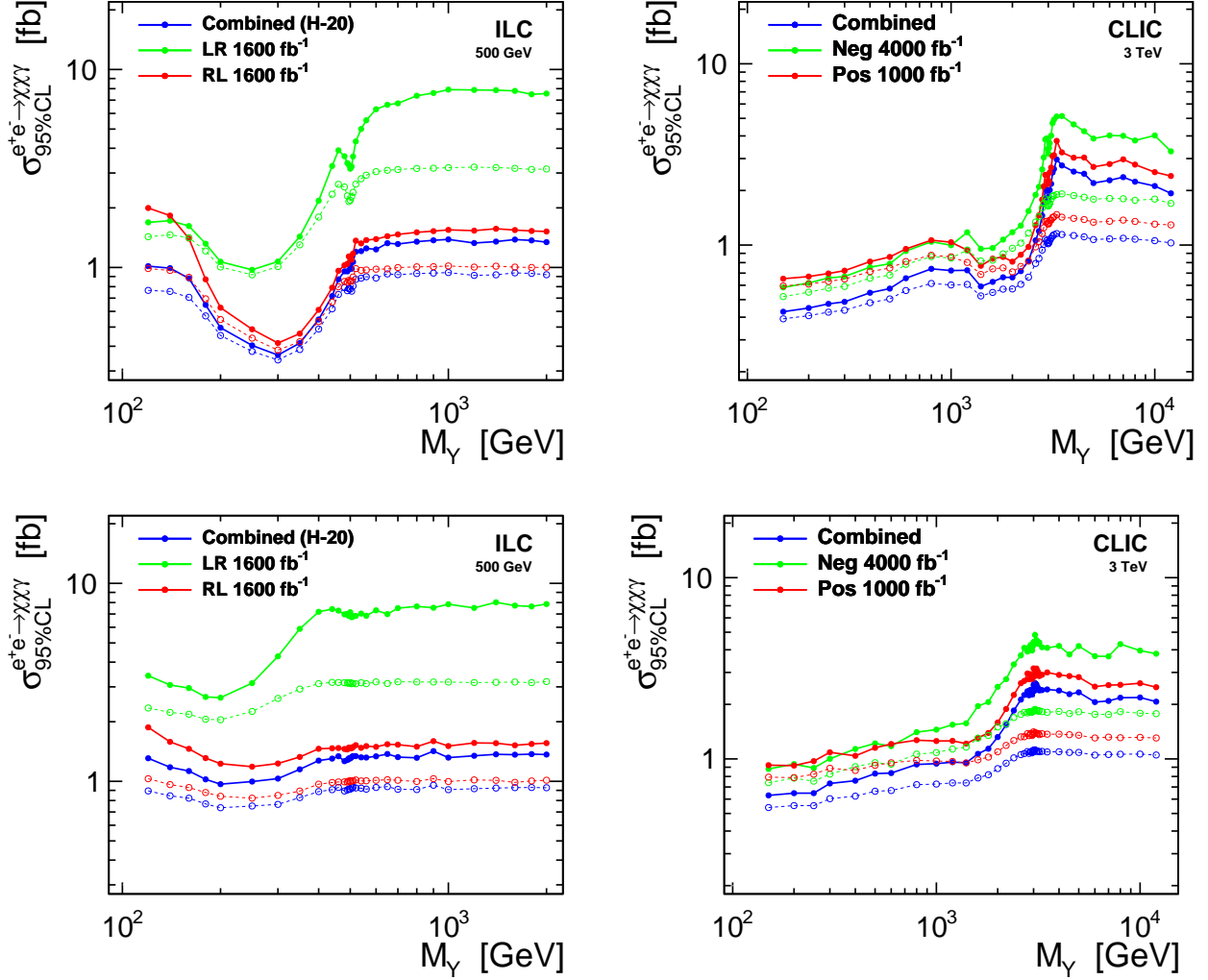


Figure 10: Limits on the cross section for the radiative light DM pair-production processes with vector mediator exchange at 500 GeV ILC (left) and 3 TeV CLIC (right). Limits extracted with (solid line) and without (dashed line) taking into account systematic uncertainties are compared for narrow mediator ( $\Gamma/M = 0.03$ ; top row) and wide mediator ( $\Gamma/M = 0.5$ ; bottom) hypotheses.

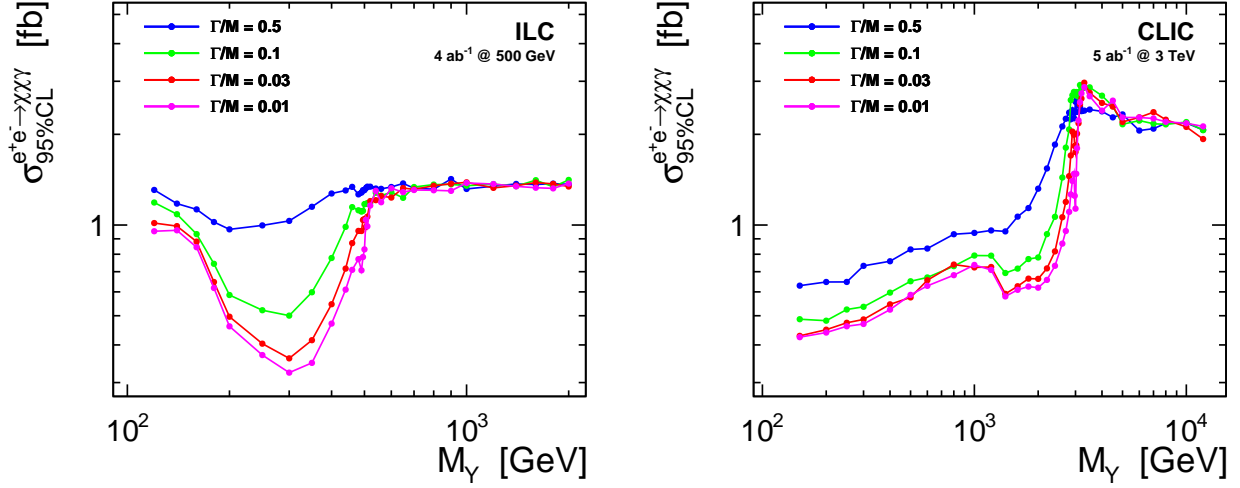


Figure 11: Limits on the cross section for the radiative DM pair-production processes with  $s$ -channel vector mediator exchange for the ILC running at 500 GeV (left) and CLIC running at 3 TeV (right) and different fractional mediator widths, as indicated in the plot. Combined limits corresponding to the assumed running scenarios are presented with systematic uncertainties taken into account.

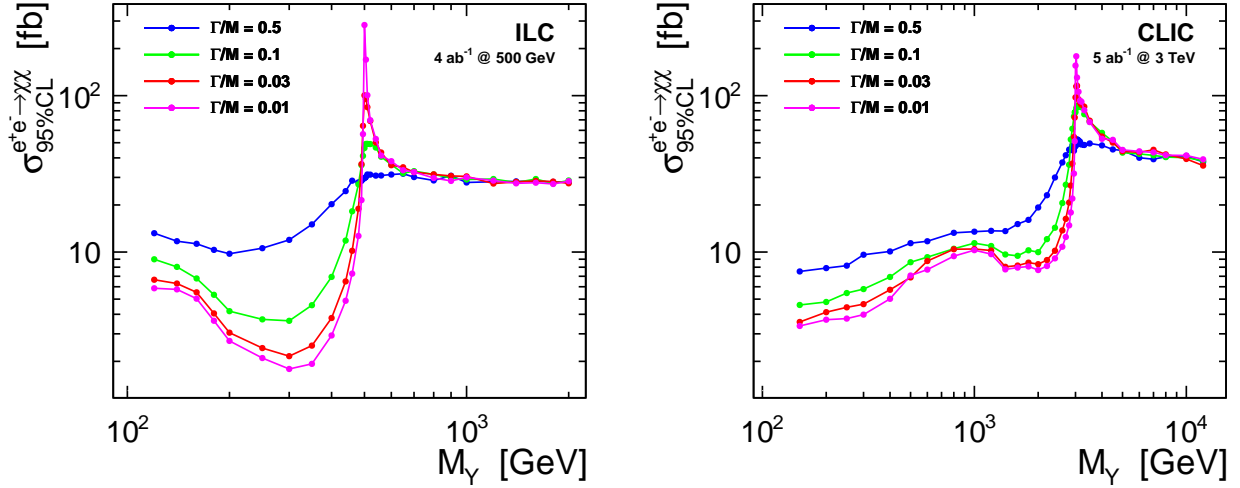


Figure 12: Limits on the cross section for light fermionic DM pair-production processes with  $s$ -channel vector mediator exchange for the ILC running at 500 GeV (left) and CLIC running at 3 TeV (right) and different fractional mediator widths, as indicated in the plot. Combined limits corresponding to the assumed running scenarios are presented with systematic uncertainties taken into account.

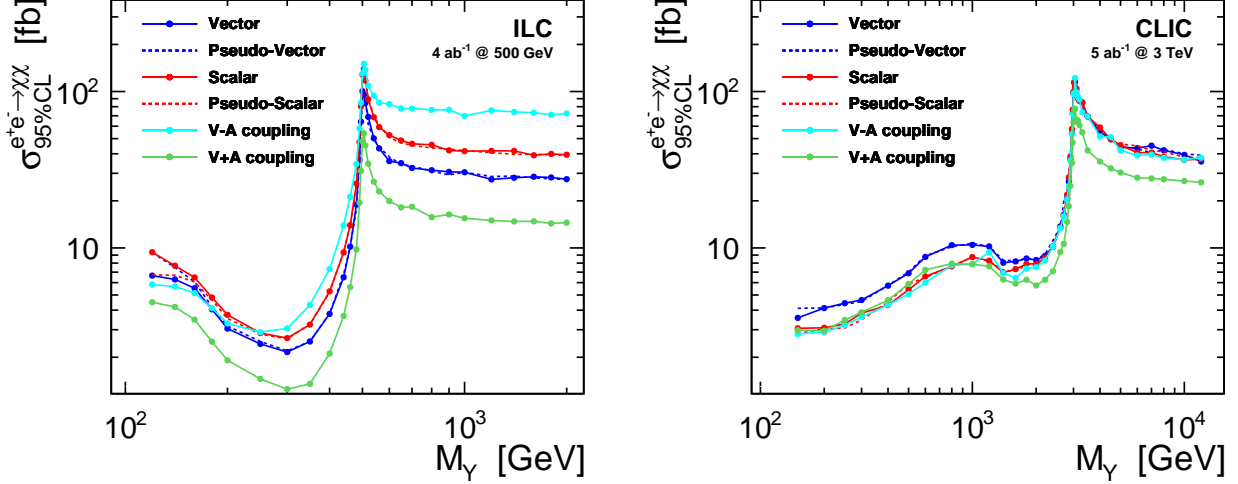


Figure 13: Limits on the cross section for light fermionic DM pair-production processes with  $s$ -channel mediator exchange for the ILC running at 500 GeV (left) and CLIC running at 3 TeV (right), for relative mediator width,  $\Gamma/M = 0.03$ , and different mediator coupling scenarios, as indicated in the plot. Combined limits corresponding to the assumed running scenarios are presented with systematic uncertainties taken into account.

ground from radiative neutrino pair-production), results in cross section limits less sensitive to mediator couplings than the ILC running scenario, where same luminosity is assumed for LR and RL configurations.

As already discussed in sec. 2.3, we assume that the mediator coupling to SM particles is small and its decays to SM particles can be neglected. The total mediator width is dominated by the invisible width resulting from its coupling to DM particle,  $g_{\chi\chi Y}$ . This coupling is thus fixed when considering a given mediator scenario by specifying mediator mass and width. This allows us to translate the extracted cross section limits to the limits on the mediator coupling to electrons,  $g_{eeY}$ , the only free model parameter after fixing the DM type, coupling structure, masses and mediator width. Limits on the mediator coupling to electrons, expected from combined analysis of ILC and CLIC data, are shown in Fig. 14 for different mediator widths. For scenarios with light mediator exchange, SM coupling limits hardly depend on the mediator width. For the Vector mediator scenario, limits of  $(1 - 4) \cdot 10^{-3}$  are expected at 500 GeV ILC, improving with mediator mass (except for the largest mediator width), while limit of about  $10^{-2}$  is expected at 3 TeV CLIC, almost independent on the mediator mass (up to kinematic limit) and width. For the width of  $\Gamma/M = 0.03$  these coupling limits correspond to the upper limits on the mediator branching ratio to electrons of about  $10^{-5}$  at 500 GeV ILC and  $10^{-4}$  at 3 TeV CLIC. This corresponds to single expected events and indicates that the analysis of mono-photon spectra gives higher sensitivity to processes with light mediator exchange than their direct searches in SM decay channels.

As shown in Fig. 15, coupling limits expected from the combined analysis of all data vary by up to a factor of 3 for ILC and up to a factor of 2 for CLIC, depending on the assumed coupling structure. The strongest limits are obtained for the V+A mediator coupling structure. For this scenario the signal cross section is largest for polarisation combinations corresponding to the lowest background levels. The weakest limits are expected for Scalar and Pseudo-scalar

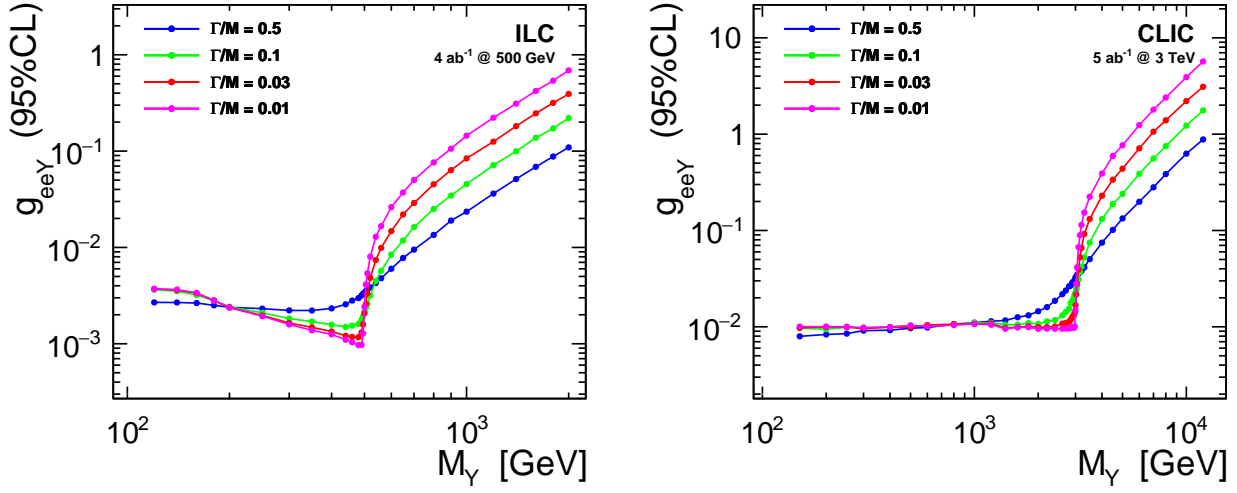


Figure 14: Limits on the vector mediator coupling to electrons for the ILC running at 500 GeV (left) and CLIC running at 3 TeV (right) and different fractional mediator widths, as indicated in the plot. Combined limits corresponding to the assumed running scenarios are presented with systematic uncertainties taken into account.

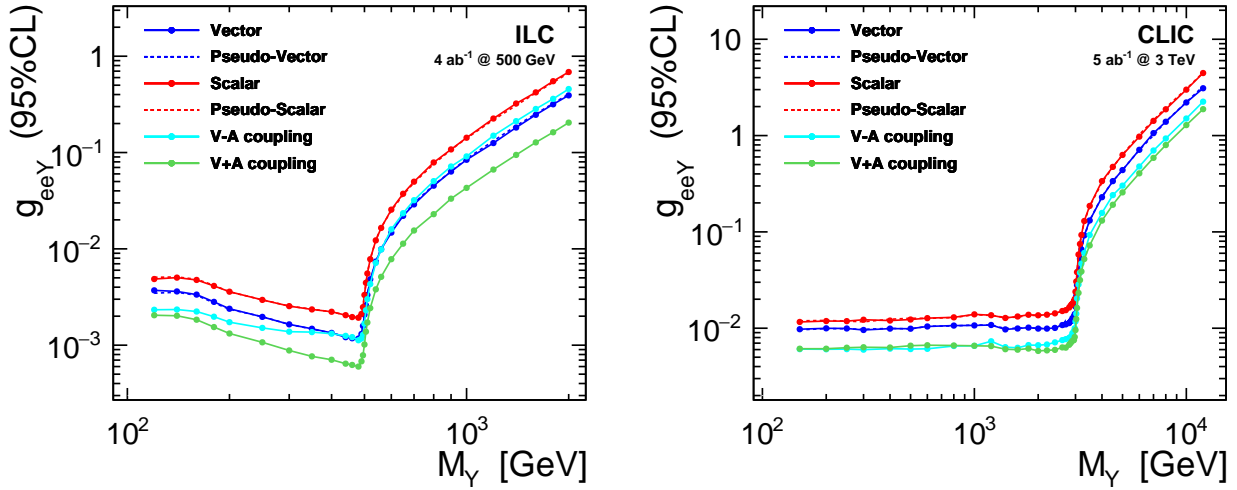


Figure 15: Limits on mediator coupling to electrons for the ILC running at 500 GeV (left) and CLIC running at 3 TeV (right), for relative mediator width,  $\Gamma/M = 0.03$ , and different mediator coupling scenarios, as indicated in the plot. Combined limits corresponding to the assumed running scenarios are presented with systematic uncertainties taken into account.

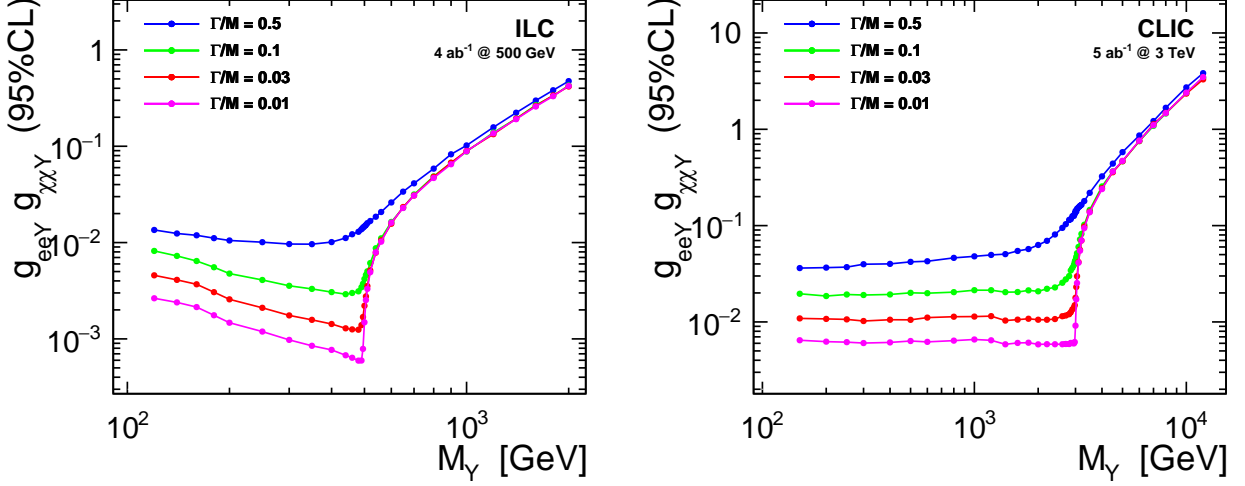


Figure 16: Limits on the product of the vector mediator couplings to electrons and to DM particles for the ILC running at 500 GeV (left) and CLIC running at 3 TeV (right) and different fractional mediator widths, as indicated in the plot. Combined limits corresponding to the assumed running scenarios are presented with systematic uncertainties taken into account. Pair-production of Dirac fermion DM is assumed.

coupling scenarios.

For heavy mediator exchange, dark matter pair-production cross section should no longer depend on the mediator width. However, results presented in Figs. 14 show strong width dependence in this mass range. This is due to the fact that mediator coupling to DM particles,  $g_{\chi\chi Y}$ , starts to be relevant for processes with exchange of heavy (virtual) mediator and, as already discussed above, this coupling is directly related to the mediator width. Width dependence is removed when limits on the product of both couplings are considered,  $g_{eeY} g_{\chi\chi Y}$ , as shown in Fig. 16. In the limit of high mediator masses,  $M_Y \gg \sqrt{s}$ , limits on the coupling product increase with square of the mediator mass. This corresponds to the fixed limit on the effective mass scale of new interactions,  $\Lambda$ , which would be obtained in the EFT approach:

$$\Lambda^2 = \frac{M_Y^2}{|g_{eeY} g_{\chi\chi Y}|}.$$

For ILC running at 500 GeV, expected EFT mass scale limits, resulting from the combined analysis of all collected data, range from about 2.6 TeV for Scalar mediator and 3.1 TeV for Vector mediator, in very good agreement with full simulation results of [3], to about 5.1 TeV for V+A mediator couplings. For CLIC running at 3 TeV, limits range from 6.1 TeV and 6.6 TeV to 10.1 TeV, respectively.

## 5 Conclusions

We propose a novel approach to estimate sensitivity of future  $e^+e^-$  colliders to pair-production of DM particles via light mediator exchange. The experimental sensitivity is defined in terms of the DM production cross section as a function of both the mediator mass and mediator width. This approach is more general and more model-independent than the approaches presented so

far, assuming given mediator coupling values to SM and DM particles. We present expected limits for pair-production of light DM particles at 500 GeV ILC and 3 TeV CLIC, based on analysis of the 2-D kinematic distributions of mono-photon events. Expected limits on the radiative DM production cross section are at the level of 1 fb and weakly depend on the assumed mediator mass and width. Limits on the total DM pair-production cross section are of the order of 10 fb except for the resonant production region,  $M_Y \sim \sqrt{s}$ , where hard photon radiation is significantly suppressed. Extracted limits on the light mediator coupling to SM particles are in the  $10^{-3} - 10^{-2}$  range up to the kinematic limit,  $M_Y \leq \sqrt{s}$ . For heavy mediator exchange, extracted cross section limits correspond to the mass scale limits up to the order of 10 TeV.

## Acknowledgements

We thank members of the CLIC detector and physics (CLICdp) collaboration and the International Large Detector (ILD) concept group for the ILC for fruitful discussions, valuable comments and suggestions. This contribution was supported by the National Science Centre, Poland, the OPUS project under contract UMO-2017/25/B/ST2/00496 (2018-2021) and the HARMONIA project under contract UMO-2015/18/M/ST2/00518 (2016-2021), and by the German Research Foundation (DFG) under grant number STO 876/4-1 and STO 876/2-2.

## References

- [1] J. de Blas et al. “The CLIC Potential for New Physics”. 3/2018 (Dec. 2018). DOI: [10.23731/CYRM-2018-003](#). arXiv: [1812.02093 \[hep-ph\]](#).
- [2] J-J. Blaising et al. “Physics performance for Dark Matter searches at  $\sqrt{s} = 3$  TeV at CLIC using mono-photons and polarised beams” (Mar. 2021). arXiv: [2103.06006 \[hep-ex\]](#).
- [3] Moritz Habermehl, Mikael Berggren, and Jenny List. “WIMP Dark Matter at the International Linear Collider”. *Phys. Rev. D* 101.7 (2020), p. 075053. DOI: [10.1103/PhysRevD.101.075053](#). arXiv: [2001.03011 \[hep-ex\]](#).
- [4] J. Kalinowski et al. “Simulating hard photon production with WHIZARD”. *Eur. Phys. J. C* 80.7 (2020), p. 634. DOI: [10.1140/epjc/s10052-020-8149-6](#). arXiv: [2004.14486 \[hep-ph\]](#).
- [5] Mauro Moretti, Thorsten Ohl, and Jurgen Reuter. “O’Mega: An Optimizing matrix element generator” (2001), pp. 1981–2009. arXiv: [hep-ph/0102195 \[hep-ph\]](#).
- [6] Wolfgang Kilian, Thorsten Ohl, and Jurgen Reuter. “WHIZARD: Simulating Multi-Particle Processes at LHC and ILC”. *Eur. Phys. J. C* 71 (2011), p. 1742. DOI: [10.1140/epjc/s10052-011-1742-y](#). arXiv: [0708.4233 \[hep-ph\]](#).
- [7] A. Heister et al. “Single photon and multiphoton production in  $e^+e^-$  collisions at  $\sqrt{s}$  up to 209-GeV”. *Eur. Phys. J. C* 28 (2003), pp. 1–13. DOI: [10.1140/epjc/s2002-01129-7](#).
- [8] J. Abdallah et al. “Photon events with missing energy in  $e^+e^-$  collisions at  $s^{**}(1/2) = 130$ -GeV to 209-GeV”. *Eur. Phys. J. C* 38 (2005), pp. 395–411. DOI: [10.1140/epjc/s2004-02051-8](#). arXiv: [hep-ex/0406019](#).

- [9] P. Achard et al. “Single photon and multiphoton events with missing energy in  $e^+e^-$  collisions at LEP”. *Phys. Lett. B* 587 (2004), pp. 16–32. DOI: [10.1016/j.physletb.2004.01.010](https://doi.org/10.1016/j.physletb.2004.01.010). arXiv: [hep-ex/0402002](https://arxiv.org/abs/hep-ex/0402002).
- [10] G. Abbiendi et al. “Photonic events with missing energy in  $e^+e^-$  collisions at  $S^{*}(1/2) = 189\text{-GeV}$ ”. *Eur. Phys. J. C* 18 (2000), pp. 253–272. DOI: [10.1007/s100520000522](https://doi.org/10.1007/s100520000522). arXiv: [hep-ex/0005002](https://arxiv.org/abs/hep-ex/0005002).
- [11] Seong Youl Choi et al. “Characterizing invisible electroweak particles through single-photon processes at high energy  $e^+e^-$  colliders”. *Phys. Rev. D* 92.9 (2015), p. 095006. DOI: [10.1103/PhysRevD.92.095006](https://doi.org/10.1103/PhysRevD.92.095006). arXiv: [1503.08538 \[hep-ph\]](https://arxiv.org/abs/1503.08538).
- [12] Neil D. Christensen and Claude Duhr. “FeynRules - Feynman rules made easy”. *Comput. Phys. Commun.* 180 (2009), pp. 1614–1641. DOI: [10.1016/j.cpc.2009.02.018](https://doi.org/10.1016/j.cpc.2009.02.018). arXiv: [0806.4194 \[hep-ph\]](https://arxiv.org/abs/0806.4194).
- [13] Adam Alloul et al. “FeynRules 2.0 - A complete toolbox for tree-level phenomenology”. *Comput. Phys. Commun.* 185 (2014), pp. 2250–2300. DOI: [10.1016/j.cpc.2014.04.012](https://doi.org/10.1016/j.cpc.2014.04.012). arXiv: [1310.1921 \[hep-ph\]](https://arxiv.org/abs/1310.1921).
- [14] Celine Degrande et al. “UFO - The Universal FeynRules Output”. *Comput. Phys. Commun.* 183 (2012), pp. 1201–1214. DOI: [10.1016/j.cpc.2012.01.022](https://doi.org/10.1016/j.cpc.2012.01.022). arXiv: [1108.2040 \[hep-ph\]](https://arxiv.org/abs/1108.2040).
- [15] Model documentation on FeynRules webpage. URL: <https://feynrules.irmp.ucl.ac.be/wiki/SimpDM>.
- [16] Andreas Albert et al. “Recommendations of the LHC Dark Matter Working Group: Comparing LHC searches for dark matter mediators in visible and invisible decay channels and calculations of the thermal relic density”. *Phys. Dark Univ.* 26 (2019), p. 100377. DOI: [10.1016/j.dark.2019.100377](https://doi.org/10.1016/j.dark.2019.100377). arXiv: [1703.05703 \[hep-ex\]](https://arxiv.org/abs/1703.05703).
- [17] Georges Aad et al. “Search for dark matter in association with an energetic photon in  $pp$  collisions at  $\sqrt{s} = 13\text{ TeV}$  with the ATLAS detector”. *JHEP* 02 (2021), p. 226. DOI: [10.1007/JHEP02\(2021\)226](https://doi.org/10.1007/JHEP02(2021)226). arXiv: [2011.05259 \[hep-ex\]](https://arxiv.org/abs/2011.05259).
- [18] Morad Aaboud et al. “Constraints on mediator-based dark matter and scalar dark energy models using  $\sqrt{s} = 13\text{ TeV}$   $pp$  collision data collected by the ATLAS detector”. *JHEP* 05 (2019), p. 142. DOI: [10.1007/JHEP05\(2019\)142](https://doi.org/10.1007/JHEP05(2019)142). arXiv: [1903.01400 \[hep-ex\]](https://arxiv.org/abs/1903.01400).
- [19] Albert M Sirunyan et al. “Search for resonant and nonresonant new phenomena in high-mass dilepton final states at  $\sqrt{s} = 13\text{ TeV}$ ” (Mar. 2021). arXiv: [2103.02708 \[hep-ex\]](https://arxiv.org/abs/2103.02708).
- [20] Philip Bambade et al. “The International Linear Collider: A Global Project” (Mar. 2019). arXiv: [1903.01629 \[hep-ex\]](https://arxiv.org/abs/1903.01629).
- [21] T. Barklow et al. “ILC Operating Scenarios” (June 2015). arXiv: [1506.07830 \[hep-ex\]](https://arxiv.org/abs/1506.07830).
- [22] “The Compact Linear Collider (CLIC) - Project Implementation Plan”. 4/2018 (Dec. 2018). Ed. by M. Aicheler et al. DOI: [10.23731/CYRM-2018-004](https://doi.org/10.23731/CYRM-2018-004). arXiv: [1903.08655 \[physics.acc-ph\]](https://arxiv.org/abs/1903.08655).
- [23] J. de Favereau et al. “DELPHES 3, A modular framework for fast simulation of a generic collider experiment”. *JHEP* 02 (2014), p. 057. DOI: [10.1007/JHEP02\(2014\)057](https://doi.org/10.1007/JHEP02(2014)057). arXiv: [1307.6346 \[hep-ex\]](https://arxiv.org/abs/1307.6346).



- [24] Emilia Leogrande et al. “A DELPHES card for the CLIC detector” (Sept. 2019). arXiv: [1909.12728 \[hep-ex\]](#).
- [25] Dominik Arominski et al. “A detector for CLIC: main parameters and performance” (Dec. 2018). arXiv: [1812.07337 \[physics.ins-det\]](#).
- [26] Halina Abramowicz et al. “International Large Detector: Interim Design Report” (Mar. 2020). arXiv: [2003.01116 \[physics.ins-det\]](#).
- [27] Moritz Habermehl. “Dark Matter at the International Linear Collider”. PhD thesis. Hamburg: Hamburg U., 2018. DOI: [10.3204/PUBDB-2018-05723](#).
- [28] Wouter Verkerke and David P. Kirkby. “The RooFit toolkit for data modeling”. *eConf* C0303241 (2003). Ed. by L. Lyons and Muge Karagoz, MOLT007. arXiv: [physics/0306116](#).
- [29] Alexander L. Read. “Presentation of search results: The CL(s) technique”. *J. Phys.* G28 (2002), pp. 2693–2704. DOI: [10.1088/0954-3899/28/10/313](#).
- [30] I. Božović Jelisavčić et al. “Luminosity measurement at ILC”. *JINST* 8 (2013), P08012. DOI: [10.1088/1748-0221/8/08/P08012](#). arXiv: [1304.4082 \[physics.acc-ph\]](#).
- [31] Strahinja Lukic et al. “Correction of beam-beam effects in luminosity measurement in the forward region at CLIC”. *JINST* 8 (2013), P05008. DOI: [10.1088/1748-0221/8/05/P05008](#). arXiv: [1301.1449 \[physics.acc-ph\]](#).
- [32] Robert Karl and Jenny List. “Polarimetry at the ILC”. *International Workshop on Future Linear Colliders*. Mar. 2017. arXiv: [1703.00214 \[hep-ex\]](#).
- [33] Graham W. Wilson. “Beam Polarization Measurement Using Single Bosons with Missing Energy”. Presented at *International Workshop on Future Linear Colliders, LCWS12*. Oct. 2012.